Performance of spatial filtering wavefront sensor for the phasing of segmented telescopes

A-L. Cheffot [ab], L. Noethe, A. Vigan [b], S. Leveque [a]
[a] European southern Observatory, Karl-Schwarzchild Strasse 2 85748 Garching bei Munchen Germany, [b] Aix Marseille Univ, CNRS, CNES, LAM, 38, rue Frédéric Joliot-Curie 13388 Marseille cedex 13, France

ABSTRACT

The next generation of extremely large telescopes requires the use of segmented mirrors. This technology needs specific wave front sensors to measure the alignment and phasing state. This paper compares two specific technologies for the measurement of phase steps between segments: a simple pin hole, and a phase contrast sensor. The efficiency of each sensor will be quantified by calculating the Fisher information, first, under ideal conditions, then including the effects of sampling and atmospheric turbulence.

1. INTRODUCTION

Currently, the only feasible technology for mirrors of the 30 meters class telescopes is segmentation. The stiffness is supplied by a control system using actuators for the rigid-body movements of the segments and edge sensors for the measurement, at high rate, of the relative heights of adjacent segments. The edge sensors need to be calibrated by optical sensors measuring the relative optical heights, from now on called phase steps, between neighbouring segments.
On the one hand, the sensor must be capable of measuring large phase steps of several micrometres after installations of segments. On the other hand, preferably also during operations to continually check the performance of the edge sensors, the optical sensor should be capable of measuring small phase steps of a few nanometres.
This paper compares two sensors that use spatial filtering in the focal plane of the telescope to convert the phase steps into intensity variations observed in the telescope exit pupil. One of them is a simple circular pinhole and the other one is a type of phase contrast sensor using a circular phase mask, that introduces a phase delay between different regions of the focal plane [1].
The theoretical comparison is based on a single phase step in the middle of a circular telescope pupil and assumes that the two segments are not tilted with respect to each other.
In the case of the pinhole the spatial filtering in the focal plane blurs the wavefront in the exit pupil. This leads to an overlap and therefore interference between the initially separated areas of the two segments. For large pinhole diameters, the blurring extends over only a small region, which leads to a modification of the signal only close to the location of the phase step, therefore generating a well localized signal. Phase differences will generate partial destructive interference, resulting in a reduced intensity at the location of the step.
In the phase contrast sensor, the expected effect is the filtering out of the low order aberration in the exit pupil plan.
The central part of the phase mask will have the same diameter as the pin hole.

Tests with the phase contrast sensor have been done in the laboratory and on sky with the APE experiment [2]. In the Zernike phase contrast Unit Sensor (ZEUS)[3], the spatial filter was a parallel plate with a circular dip in the middle. The centre of the dip was aligned in the focal plane with the optical axis of the telescope. The depth of the dip was equivalent to a phase shift of a quarter of the central wavelength of the chosen bandwidth. The phase steps were extracted from the recorded signal intensity in the exit pupil by a fit of a theoretically expected shape.

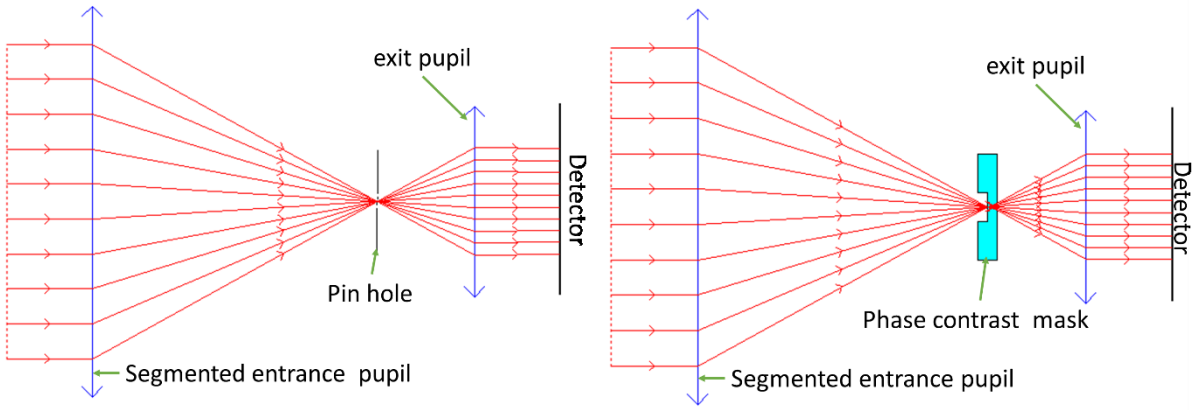

Figure 1: Simplified schematics of the two sensors, left: pinhole, right: phase contrast

For both sensors, a relatively coarse phasing can be done by modulating the phase step within a large range of several wavelengths and detecting the maximum of the coherence envelope of the signal. The coherence method has been successfully applied at the Keck [4] and on the APE test bench [5] for a Shack-Hartmann-type sensor. Also an alternative multi-wavelength methods was experimented with ZEUS [6].
For small phase steps, one can do single measurements with a narrow bandwidth, if sufficient light is available, or a broad bandwidth, if only dim stars are available.
The comparison between the two sensors in Section 3 will be done without and with taking into account atmospheric effects. Section 4 will discuss the optimal choice of the sampling for a possible use of these types of sensor in the ELT.

The comparison will be based on the study of the content of information in the signals. The chosen type of information is the Fisher information because of its close relationship to the achievable precision of measurement expressed as the rms of the measurement error.

2. THE FISHER INFORMATION AND THE CRAMER RAO LOWER BOUND

This application of the Fisher information to phase measurements has been discussed in [7] and [8]. This section only summarizes the essential features of the Fisher information.
Any information is based on the change of the signal with the variation of any parameter, in this case the phase step.
A special type of information is the Fisher information, which is defined by:

$$I(\theta) = 4 \int_{-\infty}^{+\infty} \left(\frac{\partial \sqrt{p(x|\theta)}}{\partial \theta} \right)^2 dx \,,$$

With the intensity $p(x|\theta)$ being the probability that a photon will be detected at the location x on the detector in the exit pupil, if the relative phase step is θ. Where the integrand is the Fisher information density. To make the definition valid for a single photon, the integral of $p(x|\theta)$over the pupil must be equal to 1.
The reason for the choice of the Fisher information is its link to the Cramer-Rao bound. This is the smallest error in terms of the standard deviation that you can expect in the measurement of a parameter θ. For a number $N_{photon}$of detected photons the Cramer-Rao bound (CR) is related to the Fisher information by

$$\sigma_{\mathrm{CRB}} = \frac{1}{\sqrt{I(\theta)\, N_{photon}}} \tag{1}$$

In particular for the measurement of a phase step θ the fundamental limit, irrespective of the measurement method, is given by

$$\sigma_{\mathrm{CRB}} = \frac{\lambda}{2\pi\sqrt{N_{photon}}} \tag{2}$$

All calculations will be done for one photon and a normalised Fisher information $\tilde{I}$ and a normalised Cramer-Rao bound will be defined by

$$\tilde{I} = I\left(\frac{\lambda}{2\pi}\right)^2$$

$$\tilde{\sigma}_{\mathrm{CRB}} = \sigma_{\mathrm{CRB}}\frac{2\pi}{\lambda}$$

The fundamental limit for both $\tilde{I}$ and $\tilde{\sigma}_{\mathrm{CRB}}$ for one photon will then be equal to 1.

3. CONVENTIONS

It is convenient to express the parameters in normalised form. With a being the half-diameter of the entrance pupil, λ the wavelength of the light, θ the phase step , w_m the radius of the mask in radians, r_0 the Fried parameter and x the coordinate in the pupil, we define the normalised phase step as $\tilde{\theta} = \frac{\theta}{\lambda}$, the normalised radius of the mask as $\tilde{w}_{\mathrm{m}} = w_{\mathrm{m}}\frac{2a}{\lambda}$, the normalised Fried parameter as $\tilde{r}_0 = \frac{r_0}{a}$ and the normalised pupil coordinate as $\tilde{x} = \frac{x}{a}$.
To obtain the maximum of information, the optimum diameter $2\tilde{w}_{\mathrm{m}}$ of the phase mask is approximately 1,5 times the diameter of the image in the focal plane [8].With atmospheric turbulences included, in normalised parameters this translates to $\tilde{w}_{\mathrm{m}} \approx \frac{1{,}5}{\tilde{r}_0}$.
For the discussion of the performance of the two sensors related to the measurement of phase steps, we will consider parameters that are suitable for measurements on a 40 m class telescope. For example, if the seeing is improved in the ELT by the adaptive M4, one may expect a Fried parameter of the order of $r_0 \approx 400$ mm. With an aperture radius of 20 m this gives $\tilde{r}_0 \approx 0{,}02$ and, consequently, $\tilde{w}_{\mathrm{m}} \approx 75$.
For the phase contrast sensor the best phase delay by the inner part of the mask is $\frac{\lambda}{4}$ [9]. This phase delay will be used in all calculations.
All calculations are done for monochromatic light and no gap between the segments. The result are obtained with semi-analytical and fast Fourier transform calculations.

4. SIGNALS

Figure 2**Error! Reference source not found.** and Figure 3 show typical signals for the two sensors without atmospheric disturbances for various phase steps. The plots on the left across the whole pupil are done with $\tilde{w}_m = 20$ since with $\tilde{w}_m = 75$ the wiggles away from the centre are hardly visible. The plots on the right with the a narrow range around the centre are done with $\tilde{w}_m = 75$.

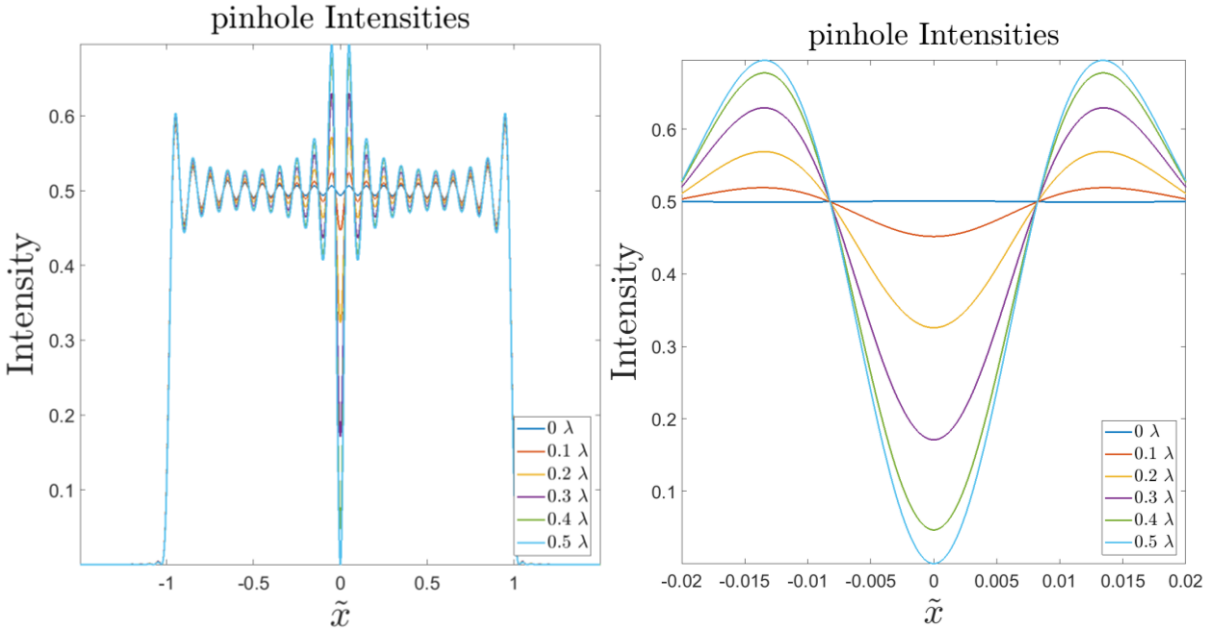

Figure 2: Typical signals for various phase steps for the pinhole sensor without atmosphere. Left: full pupil with $\tilde{w}_m = 20$, right : central section with $\tilde{w}_m = 75$

The plots on the left hand side of Figure 2 and Figure 3 show that for both sensors there are approximately $\tilde{w}_m$ maxima across the pupil. However, the signals related to the phase steps are well localized around the centre of the pupil.

For the pinhole and large radii $\tilde{w}_m$ of the pinhole in units of $\frac{\lambda}{2a}$, the value at $\tilde{x} = 0$ is approximately $0.5 \cos^2 \tilde{\theta}$.

Since the signal of the pinhole sensor is always symmetric around $\tilde{x} = 0$, the sign of the phase step is not detectable.

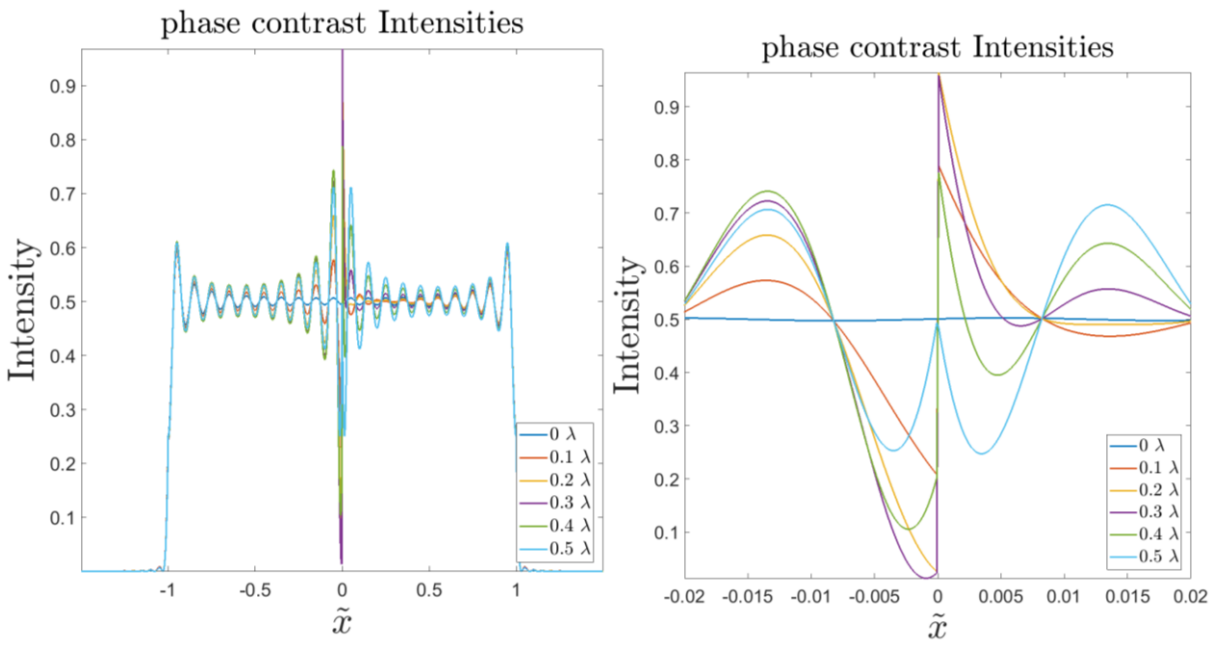

Figure 3: Typical signals for various phase steps for the phase contrast sensor without atmosphere. Left: full pupil with $\tilde{w}_m = \mathbf{20}$, right : central section with $\tilde{w}_m = \mathbf{75}$

The signal of the phase contrast sensor without atmosphere, shown in Figure 3, with a phase delay of the mask of $\frac{\lambda}{4}$, is more complex than the one of the pinhole sensor. In general, it is a superposition of a symmetric and an antisymmetric signal. Because of the asymmetry of the signals, in particular for small phase steps, one can detect the sign of the phase steps.
Apparently, the coordinates of the zeroes of the signals are independent of the phase step.
Figure 4 shows the intensities, with the atmosphere, for $\tilde{r}_0 = 0.02$ and $\tilde{w}_m = 75$. Qualitatively, the signals are quite similar to the ones without the atmosphere. Also, the coordinates of the zeroes are still independent of the phase step, however they are approximately 20% bigger than the ones without atmosphere.

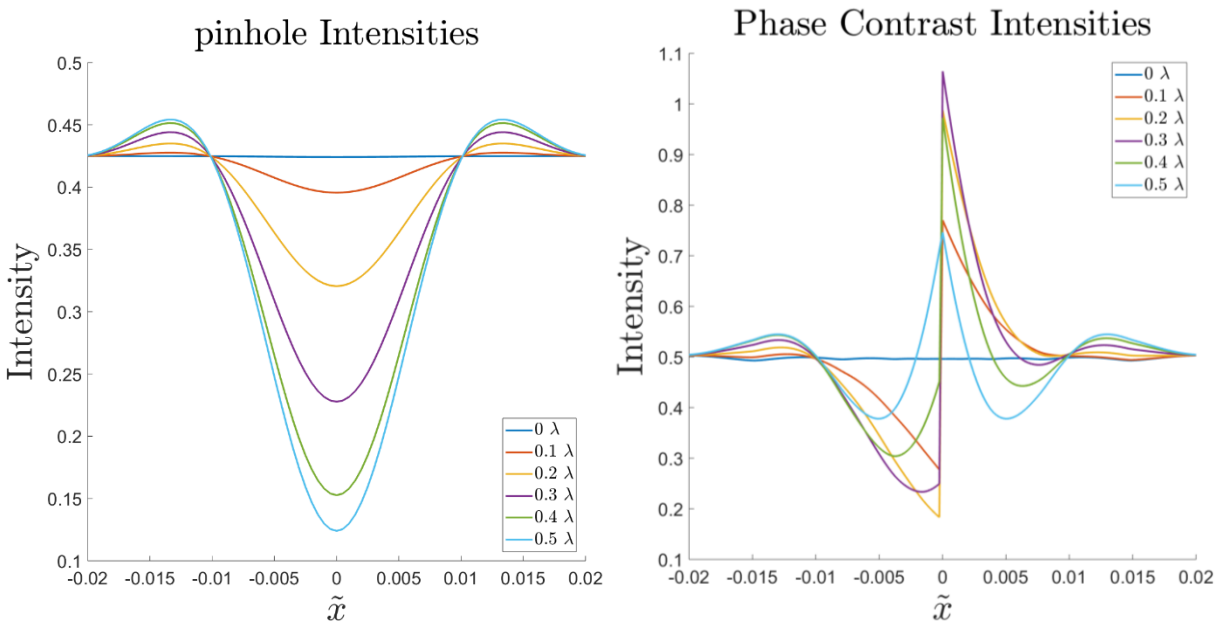

Figure 4: typical signals with atmosphere ($\tilde{r}_0 = 0.02$ and $\tilde{w}_m = 75$). Left: pinhole, right: phase contrast

5. FISHER INFORMATION

Figure 5 shows the Fisher information densities without atmosphere.
Apparently, for the pinhole sensor, the Fisher information densities are zero for $\tilde{\theta} = 0$ and $\tilde{\theta} = 0{,}5$. This is consistent with the intensities to $x = 0$ being equal to $0.5\cos^2\tilde{\theta}$, since $\sqrt{p(\tilde{x}|\tilde{\theta})} \propto \cos\tilde{\theta}$ and therefore $\frac{\partial}{\partial\tilde{\theta}}\sqrt{p(\tilde{x}|\tilde{\theta})} \propto \sin\tilde{\theta}$. Contrary, the Fisher information densities of the phase contrast sensor are always non-zero and roughly of the same order of magnitude for all phase steps.

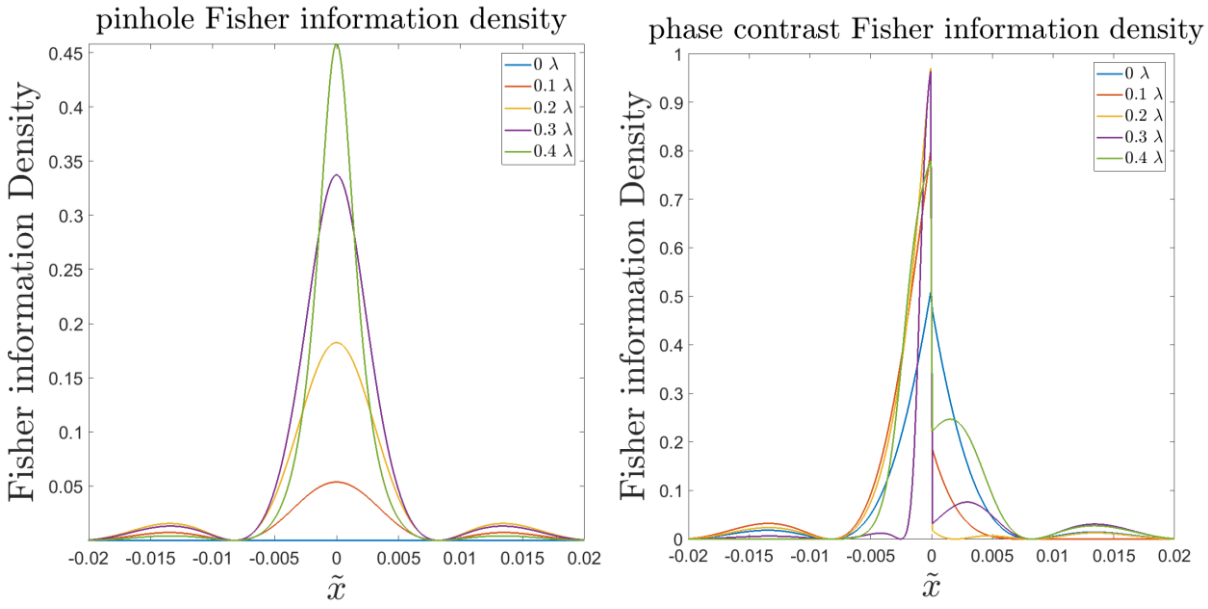

Figure 5: Fisher information densities for various normalised phase steps and no atmospheric disturbances.

Figure 6 shows the Fisher information densities with the atmosphere, for $\tilde{r}_0 = 0.02$. Qualitatively, they are rather similar to the ones without atmospheric disturbances. However, the values are about 50% smaller.

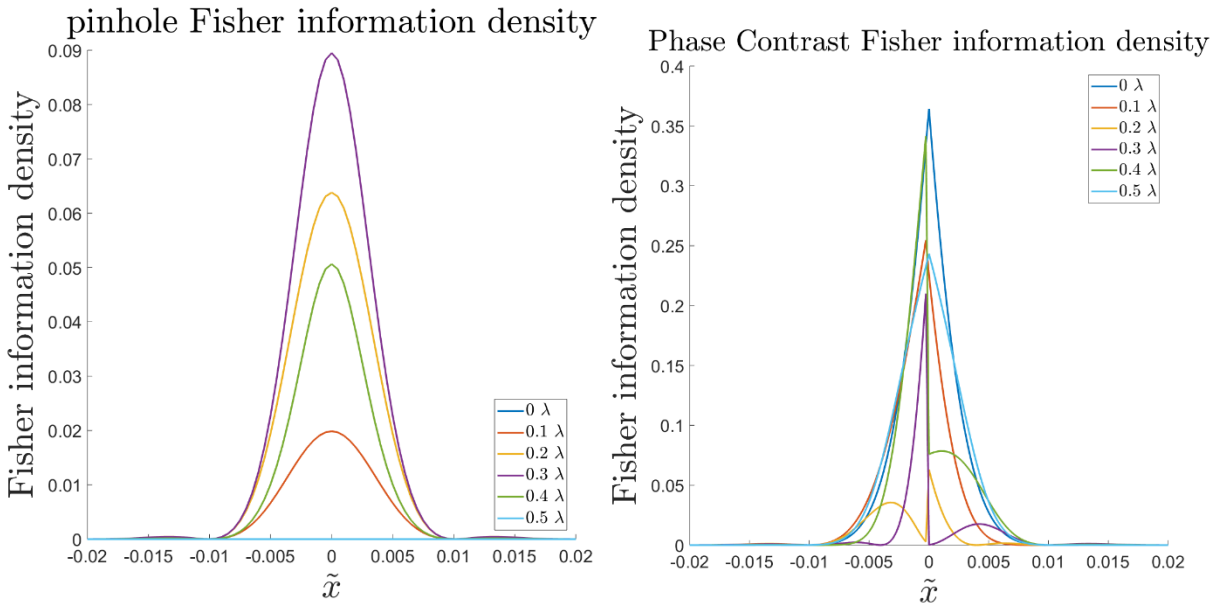

Figure 6: Fisher information densities for various normalised phase steps and $\tilde{\boldsymbol{r}}_{\boldsymbol{0}} = \mathbf{0,02}$.

Figure 7 shows, for both sensors, the normalised Fisher information $\tilde{I}$ as a function of the phase step, with $\widetilde{w}_{\mathrm{m}} \approx 75$, without atmospheric disturbances as well as with a seeing of $\tilde{r}_0 = 0.02$. As already mentioned above, the major difference between the two sensors is that the phase contrast sensor is sensitive, although with significant variations, for all phase steps, whereas the sensitivity

of the pinhole sensor converges to 0 for $\tilde{\theta} \to 0$ and $\tilde{\theta} \to \frac{1}{2}$. This means that for these two phase steps, the signal does not vary with a change of the phase step. Consequently, the pinhole sensor cannot measure small phase steps and phase steps around $\frac{\lambda}{2}$. Surprisingly, for phase steps around 0.27λ, the pinhole sensor is more sensitive than the phase contrast sensor.

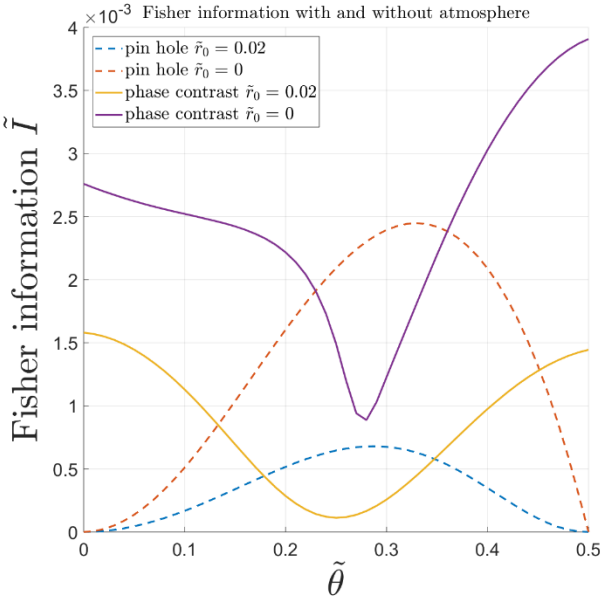

Figure 7: Normalised Fisher information for both sensors, without and with atmospheric disturbances.

Qualitatively, for both sensors, the dependence of $\tilde{I}$ on the phase step is rather independent of the seeing conditions. The Fisher information is largely determined by diameter of the mask. A seeing with $r_0 \approx 400\text{mm}$ reduces $\tilde{I}$ only by roughly a factor of 2.

6. SIGNAL WIDTH

For Figure 2, Figure 3 and Figure 4, the width of a signal could be defined as the distance between the first common zeroes of the signals for all phase steps to both sides of the centre. For all values $\widetilde{w}_\text{m}$, particularly for large values of $\widetilde{w}_\text{m}$, these zeroes are approximately at $0{,}615/\widetilde{w}_\text{m}$. The signal width does not change strongly with the seeing. For a seeing with $r_0 \approx 400\text{mm}$ it only increases by 25%.

A similar way to define the signal width would be the distance between the first zeroes of the Fisher information density around the centre, which coincide with the zeroes of the intensities. However, visually the Fisher information densities are more concentrated towards the centre than the intensities.

7. OPTIMAL SAMPLING FOR PHASING WITH PHASE MASK

The sampling is defined as the number of pixels across the signal width Δx. All the previous results were obtained with simulations using samplings that were much better than realistic samplings.

With a working wavelength of 0.65 µm and a pin hole diameter of 1", the signal width is approximately 165 mm. For a segment size of 1420 mm edge to edge the signal width is approximately 1/10 of a segment.
For the ELT, there are 39 segments across the diameter, including a central obstruction equivalent to 9 segments. The image of the 39 segments must to fit onto the camera, while providing sufficient sampling for the signal. In [1] the recommendation is to use 4 points across the signal width. This means the detector must have at least $4 \cdot 10 \cdot 39 \approx 1600$ pixels in one direction.
Figure 8 shows, for both sensors, the dependence of the Fisher information on the sampling. The Fisher information will also depend on the pixel position relative to the centre. The dashed lines in Figure 8 shows the minima and maxima of the Fisher information for several pixel positions, and the solid line is the average over all of these positions. For an estimate of the effect of the sampling one should always take the minimum value.
The pinhole sensor is much less sensitive to an under-sampling than the phase contrast sensor. The major reason for this is the difference in the symmetries of the signals.
For the pinhole sensor, a sampling of 4 decreases the Fisher information with respect to and infinite sampling, by approximately 6%, which is equivalent to an increase of the Cramer-Rao bound be of the order of 3%. There is no difference between minima and maxima down to a sampling of 3.
With the phase contrast sensor, a sampling of 4 decreases the minimum of the Fisher information by approximately 60%, which is equivalent to an increase of the Cramer Rao bound by ≈ 60%.
Apparently, the limits for infinite sampling are only approached for samplings of approximately 40 across the signal width.

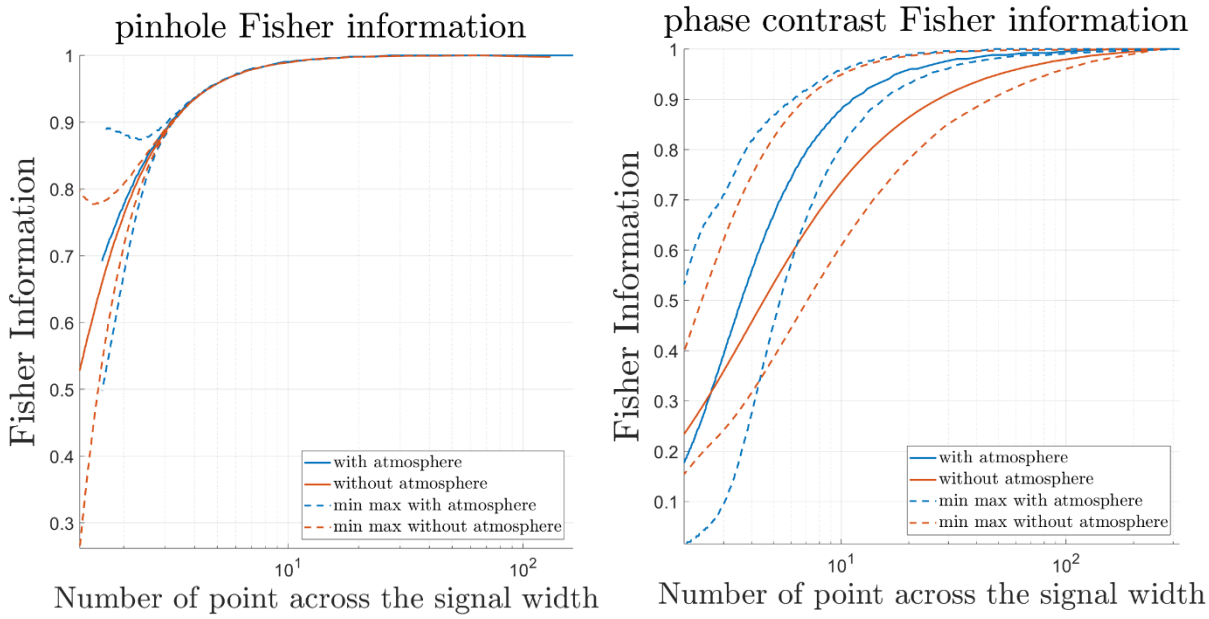

Figure 8: Fisher information with $\widetilde{\boldsymbol{w}}_{\mathrm{m}} \approx \mathbf{75}$ and $\widetilde{\boldsymbol{\theta}} = \mathbf{0.2}$ for different signal sampling with atmosphere correspond to . : $\tilde{\boldsymbol{r}}_{\mathbf{0}} = \mathbf{0,02}$ Left: pinhole, right: phase contrast

8. FEASIBILITY FOR PHASE STEP MEASUREMENT IN THE ELT

The pinhole sensor may, despite its low sensitivity for small phase steps, be feasible for coarse phasing, that is measurements with the envelope method, using phase steps over a large range.
However, for measurements of small phase steps, without disrupting the wavefront, the pinhole sensor is not suitable because of its low sensitivity for small steps and its symmetry with respect to the sign of the step.
On the contrary the phase contrast sensor does not suffer from this limitations. In particular, if continuous or frequent measurements of usually small phase steps during observations were envisaged, the phase contrast sensor is very promising. In this case only rather dim reference stars would be available, which requires the Fisher information to be as large as possible.
As an example, with a sampling of 4 pixels across the signal width, $\widetilde{w}_{\mathrm{m}} \approx 75$ and $\tilde{r}_0 = 0{,}02$, the normalised Fisher information would be, according to figures Figure 7 and Figure 8, of the order of $0{,}001$. With a broadband measurement with a bandwidth of 300 nm, according to the behaviour of the Shack-Hartmann sensor [7], this might be reduced to $0{,}0005$, equivalent to $\sigma_{CRB} \approx 50\frac{\lambda}{2\pi} \approx 5\ \mu m$ for one photon.
Reducing this to 10 nm would require a total number of photons across a band with a width of the order of the length of the edge of approximately $2{,}5 \cdot 10^5$. Even assuming that only 20% of the star light reaches the sensor, this could be achieved with a star of magnitude 16.
This estimate is fully in line with on-sky measurements on the APE experiment [8], where the ZEUS sensor measured phase steps with errors of 20 nm rms with stars of magnitude 15 despite the strong limitations of the detector.
In addition to the above, the phase contrast sensor has the possibility to recognize the sign of the phase step. This is not possible with the pinhole sensor because of its symmetric signal.

9. BIBLIOGRAPHY

[1] Surdej, I., Yaitskova, N. and Gonte, F. (2010). On-sky performance of the Zernike phase contrast sensor for the phasing of segmented telescopes. Applied Optics, 49(21), p.4053.

[2] Gonte, F., Yaitskova, N., Derie, F., Constanza, A., Brast, R., Buzzoni, B., Delabre, B., Dierickx, P., Dupuy, C., Esteves, R., Frank, C., Guisard, S., Karban, R., Koenig, E., Kolb, J., Nylund, M., Noethe, L., Surdej, I., Courteville, A., Wilhelm, R., Montoya, L., Reyes, M., Esposito, S., Pinna, E., Dohlen, K., Ferrari, M. and Langlois, M. (2005). APE: the Active Phasing Experiment to test new control system and phasing technology for a European Extremely Large Optical Telescope. Advanced Wavefront Control: Methods, Devices, and Applications III.

[3] Dohlen, K., Langlois, M., Lanzoni, P., Mazzanti, S., Vigan, A., Montoya, L., Hernandez, E., Reyes, M., Surdej, I. and Yaitskova, N. (2006). ZEUS: a cophasing sensor based on the Zernike phase contrast method. Ground-based and Airborne Telescopes.

[4] Chanan, G., Troy, M., Dekens, F., Michaels, S., Nelson, J., Mast, T. and Kirkman, D. (1998). Phasing the mirror segments of the Keck telescopes: the broadband phasing algorithm. Applied Optics, 37(1), p.140.

[5] Gonte, F., Mazzoleni, R., Surdej, I., Noethe, L., "On-sky performances of an optical phasing sensor based on a cylindrical lenslet array for segmented telescopes", Applied Optics 50(12), 1660 (2011).

[6] Vigan, A., Dohlen, K., Mazzanti, S., "On-sky multiwavelength phasing of segmented telescopes with the Zernike phase contrast sensor", Applied Optics 50(17), 2708 (2011).

[7] Noethe, L., Adorf, H., "Optical measurements of phase steps in segmented mirrors—fundamental precision limits", Journal of Modern Optics 54(1), 3-31 (2007).

[8] Surdej, I. (2011). Co-phasing segmented mirrors: theory, laboratory experiments and measurements on sky. Ph.D Thesis. Fakultat fur Physik der Ludwig-Maximilians-Universitat Munchen.

[9] Yaitskova, N., Dohlen, K., Dierickx, P. and Montoya, L. (2005). Mach–Zehnder interferometer for piston and tip–tilt sensing in segmented telescopes: theory and analytical treatment. Journal of the Optical Society of America A, 22(6), p.1093.